International Journal of
Science and Engineering Investigations
vol. 6, issue 63, April 2017
ISSN: 2251-8843

A Novel Method of Studying Colloidal Particles, on the Example of Lignin-Diesel Fuel System

Ivan Reznikov
Belarusian State University
(ivanreznikov@gmail.com)

***Abstract*-** The knowledge of the colloidal particle structure and the nature of aggregation processes can hardly be overestimated due to the importance of the field: ceramics, pigments, catalysis, etc. In this paper photogrammetry-a method of computer vision, was applied for studying colloidal aggregates, based on lignin-diesel fuel dispersions. The suggestion about the layer structure of the obtained aggregates was proved with the methods of mathematical processing, by distinguishing the three main color intensities (Red, Magenta, Yellow), followed by stage-separation process. The number of layers on a par with the ratio of the components of the colloid system was calculated for a set of 25 images, resulting in obtaining similarity with micelle structures. The content of the dispersed phase 40.86±0.34 % correlates with capillary-saturated value obtained in previous studies. The dispersion phase content within the layers allowed correlating the experiment with the diffusion limited aggregation theory. The aggregation process was also noted on the SEM photographs.

***Keywords*-** *Colloidal Particle, Photogrammetry, Lignin-Diesel Fuel*

I. INTRODUCTION

Development of photogrammetry from the advent of photography as means of obtaining images until recently came mainly through the problems arising during ground surveys and aerial photography for mapping purposes. The use of photogrammetry for measurement of closely spaced objects (engineering photogrammetry) was limited by expensive needs and low productivity of the analog measuring equipment (stereocomparators, etc.).

However, the spread of high-performance computing on one hand, and improving the means of digital imaging, on the other hand, led to necessary preconditions for the emergence of high-performance digital hardware and software systems for practical engineering photogrammetry. In recent decades it became possible to apply the methods of computer vision for solving non-contact measurements and creating three-dimensional computer models of complex objects, providing high accuracy and high degree of automation of measurements in industry and manufacturing.

At present time image processing and analysis are increasingly used in various fields of industry and everyday life. These include face and barcode detection, development of various security systems, satellite data processing, new technologies for handling documents and many others. Image interpretation is widely used in science, namely in geology [1] and aerial photography [2], in medicine detecting cancer [3], in intracoronary ultrasound [4] and dental care [5], in chemistry using electron microscopy [6] and studying electrophoresis gels [7] for 3D modeling [8], etc. Image processing is used in biology and medicine [9] in physics and chemistry [10-11].

In this study the method of microscopic image analysis is applied to investigate the mechanism of particle aggregation in colloid systems. The importance of the mechanism of agglomeration or aggregation of small particles in order to form larger structures as clusters and the colloid particle structure is important both scientifically and technologically and established in producing monodisperse colloids, colloid crystals growth, in water treatment, ceramics, etc [12].

II. THE APPROACH

A. Color models

A color model is an abstract thing, in which color is represented as a set of numbers. The main task of color models is the color to be unified. Color models define the specific coordinate system, which can uniquely determine the color. Each of these models has its own pros and cons.

Each model was obtained by certain calculation according to [13].

1) RGB model

From Grassman's laws of additive color mixture an idea of the additive (based on color mixing directly from emitting objects) model of color reproduction is appeared. Every color is a mix of red, green and blue. If we denote these color points on the graph, then the whole set of colors that can be obtained by mixing them, will be inside a triangle. And its area is much less than the range of colors that can be distinguished.

2) CMY model

Subtractive model CMY (cyan, magenta, yellow) is used to obtain hard copy (print) images, and in some ways is the

opposite of the color RGB-cube. If the model RGB basic colors - the colors of the light sources, the model CMY – is a model of absorption colors.

3) HSB and HSL models

The difference between HSB and HSL model is that brightness in the HSB model changes from black to the brightest white, whereas lightness in the HSL model can be changed the lightness of the color from black to white, without changing saturation.

4) CIE XYZ and CIE Lab models

The International Commission on Illumination (CIE) has a system where, each color corresponds with a certain ratio of imaginary primary colors: X (imaginary red), Y (imaginary green), Z (imaginary blue) were developed. A (x,y) pair is enough to set a variety of colors. To set the brightness the third axis z is needed. The main aim of CIE Lab was to eliminate the nonlinearity of the CIE XYZ. CIE Lab model was calculated according to the method, described in [14]

5) YIQ and YUV

In the YIQ and YUV color system color information is presented as a brightness signal (Y) and two color difference signals (IQ and UV respectively). An important advantage of this method is the separation of information about the color and brightness of the image.

B. Materials

The hydrophobized acid hydrolysis lignin was produced by the Bobryisk's plant for biotechnologies (Belarus) was used. The moisture content of the sample was 7.0±0.4%, the packed density — 240 kg/m^3, the absolute density for helium — 1480 kg/m^3, the specific surface area for nitrogen — 3000 m^2/kg and the total volume of pores — $4.5 \cdot 10^{-5}$ m^3/kg. The size distribution of the investigated particles can be described Gaussian curves, $D_x50 = 93.8$ mkm, $3\sigma = 6.7$ mkm.

DF has the density of 800 kg/m^3, surface tension — $30.8 \cdot 10^3$ N/m, viscosity — 9.45 mPa·s.

C. Experimental details

Dispersions of lignin, an organic polymer found in plant tissue in diesel fuel (DF) with a content of lignin from 10 to 40% were prepared by the gravimetric method with subsequent agitation in an IKA WERKE mechanical impeller agitator (Germany) for 10 min with a velocity of 500 rpm.

In this study several tracing programs were used for tracing images:

- Adobe Illustrator (Adobe)
- Neuro Tracer (Brand Security Systems GmbH)
- Vextractor (VextraSoft)

It analyzes the color pixel of the original image, and then allocates a predetermined amount of pixels between the groups so that the color in each of them was close to each other. For each of the groups the most characteristic color is defined. After that the boundaries of the area (or areas), composed of pixels of each group are constructed. Finally, the polygons filled with relevant characteristic color are drawn within the constructed boundaries.

Tracing regime included color threshold (CT1), minimum pixel area (MPA), curve fit and corner threshold (Adobe Illustrator) and color tolerance (CT2), gradient threshold (GT) and smoothing factor (Vextractor). Setting smoothing factor (Vextractor) the same as curve fit parameter (Adobe Illustrator), CT1 and MPA were correlated with CT2 and GT respectively. The curve fit and corner threshold were set at "normal" value, smoothing factor remained default value, whereas the values of CT1, CT2, MPA and GT were varied.

D. Measurements

1) Image Acquisition

For imaging, the colloid lignin-diesel fuel system was placed on the glass slide on the stage of the optical microscope Amplival with Carl Zeiss lens. Individual colloid particles were found in excess of the dispersion medium. A 6.0 megapixel digital camera Canon Power Shot A540 was positioned instead of one of the eyepieces. The gained images with a resolution 2816x2112 had a scale of 1:25 and were saved in JPEG format (24 bits).

2) Particles size distribution

Laser scattering method was used for dispersion analysis of lignin. The measurement of particle size was performed on Mastersizer 3000 together with Aero S disperser (both – "Malvern"). SEM technique

The particles' and agglomerates' surface morphology was investigated by LEO-1420 scanning electron microscope (Carl Zeiss, Germany). A gold layer of 10 nm thickness was sputtered on the particles' surface to eliminate the electric charging of the sample. The operating voltage was 20 kV.

3) Zeta potential measurement

The Zeta potential values were determined by using a Zeta-Meter 3.0+ (USA) and ZetaProbe Analyzer (USA). For measurements using the Zeta-Meter 3.0+, samples were dispersed in diesel fuel (pH 5.62).

III. Results and Discussions

In order to study the physical properties of individual colloid particles, a section of a separate particle was investigated, according to Figure 1. The diagonal AB was chosen, as it contains information about the agglomerate structure. The RGB values of pixels were the analytical signals in this study.

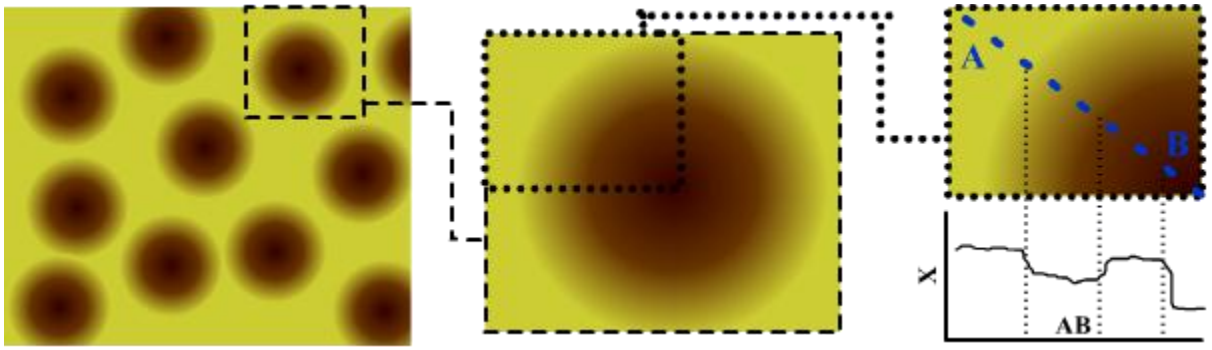

Figure 1. Illustration of the investigated method

A set of 25 images was studied. For simplicity, the investigation method is shown for only one image, whereas the conclusions are based on statistical calculations of the whole set.

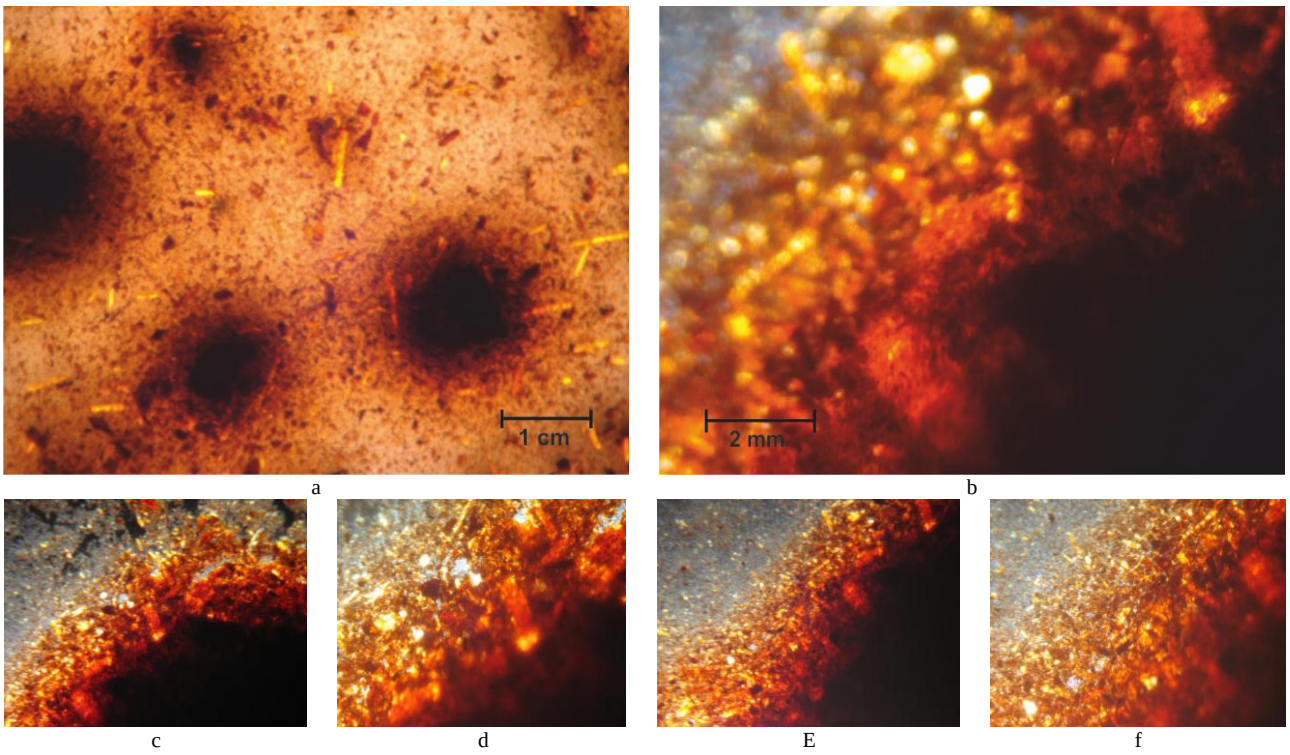

Figure 2. Images of lignin – DF colloid aggregates

RGB and CMY color channels were extracted from the selected image. The intensities of selected colors on the diagonal AB are presented with corresponding histograms in figure 3.

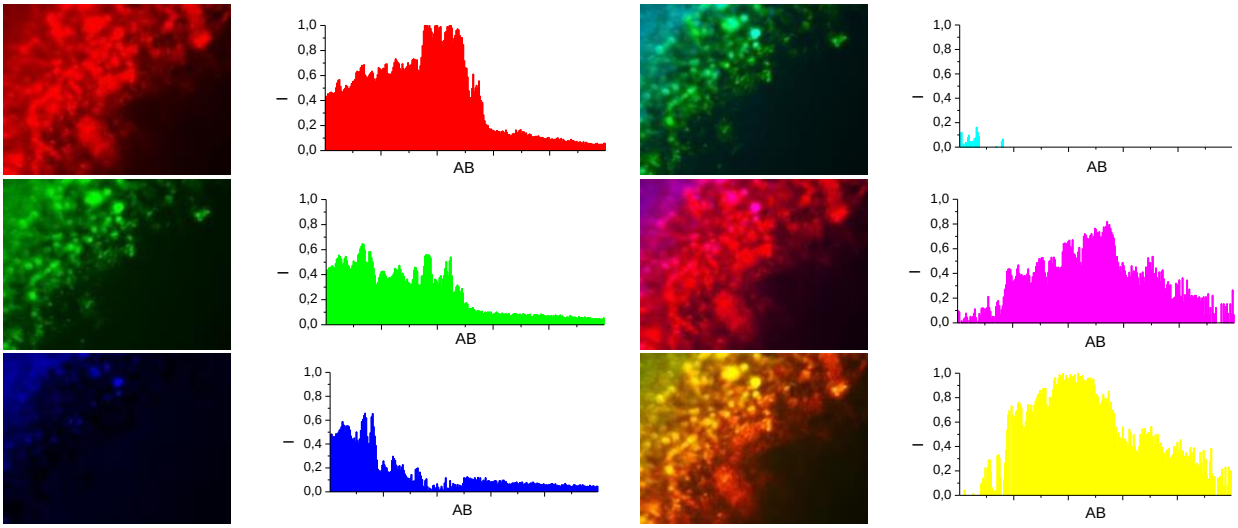

Figure 3. RGB and CMY color distribution of the Figure 2b photo

In order to find the correlation between pixel values and lignin-DF ratio the most intensive color channels were selected according to the total intensity value (Table 1).

TABLE I. INTENSITY OF COLORS ON FIGURE 2B

	Red	Green	Blue	Cyan	Magenta	Yellow
$\sum_{i=k}^{N} S_i$	107.86	63.08	40.22	1.23	87.23	121.57

The digital camera can be used as a spectrophotometer [15]. The Beer–Lambert law is exponential:

$$I = I_o e^{-\chi_\lambda Cl} \quad (1)$$

This equation is a monotonic, whereas the values of the color intensities undergo kinks. Nevertheless an increase in the lignin content is agreed with an increase in the color intensity. The content of lignin varies not continuous, but discrete, what is likely for colloid particles [16]. The image was traced in order to normalize the values of the color intensities, where a sharp change in color values represents a transition to the next layer, with other lignin-DF ratio.

Due to fact, that the values vary nonmonotonic, increasing (part I) and decreasing part (part II) of the data of the most intensive colors Red, Magenta and Yellow were analyzed separately. The nonmonotonic behavior for color models can be explained by the limitations of the color spectrum of RGB, CMY and other color models based on them (Figure 4). The blue color of the DF was obtained using the polarizing ability of the microscope to clearly separate the outer boundary of the agglomerate. It was found, that moving along the AB diagonal at certain point P' the values of G,B,C has a local maximum followed by rapid decrease, whereas the values of M and Y has a local minimum, followed by rapid increase.

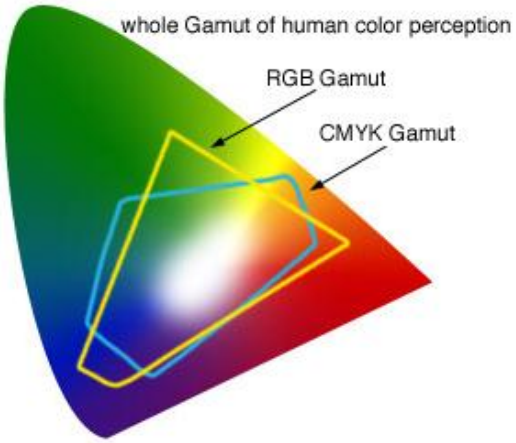

Figure 4. Illustration of different gamuts (https://ic.arc.losrios.edu)

Continuing moving on diagonal AB, a point P'', where the values of Green, Blue has a local maximum followed by rapid decrease, whereas the values of Red, Magenta and Yellow has a local minimum, followed by rapid increase. The third point P''' is mark at a pixel, where the values of the two most intensive colors Red, Magenta and Yellow sharply decrease. This analysis allows dividing part I of the Red, Magenta and Yellow histogram on three parts or stages. The number of intervals on part I is distinguishable from the CIE XYZ, CIE Lab, CIE Luv, Msh histograms (Table 2). Stage 1 represents the interval from 0 to P', stage 2 — from P' to P'' and stage 3- from P'' to P''' (Figure 5).

TABLE II. COLOR DISTRIBUTION OF THE CIE XYZ, CIE LAB, MSH AND CIE LUV MODELS OF THE FIGURE 2B PHOTO

CIE XYZ	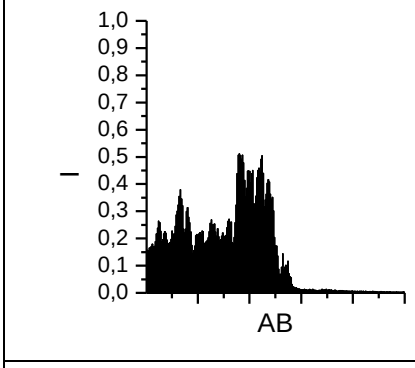	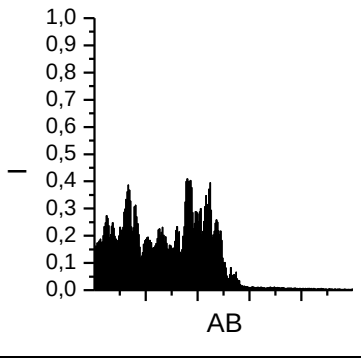	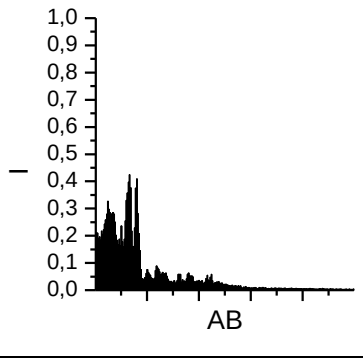
	X	*Y*	*Z*
CIE Lab	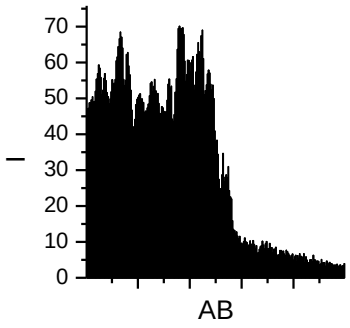	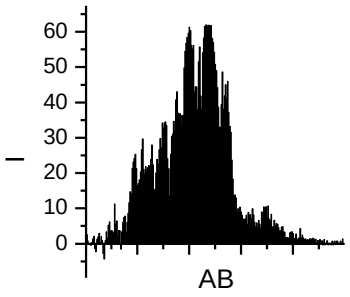	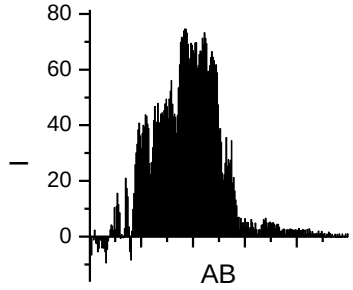
	*CIE-L**	*CIE-a**	*CIE-b**
Msh	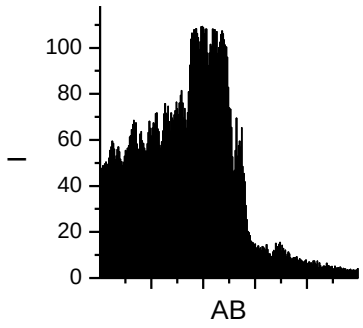	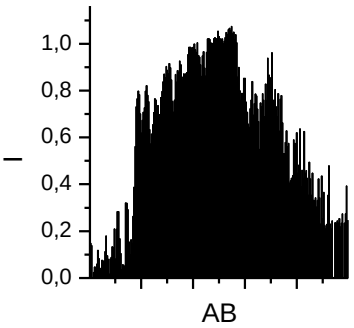	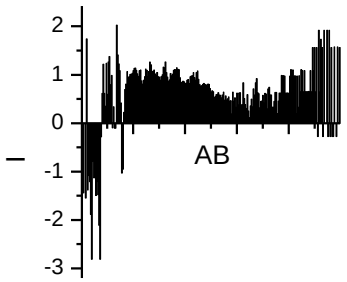
	M	*s*	*h*
CIE Luv	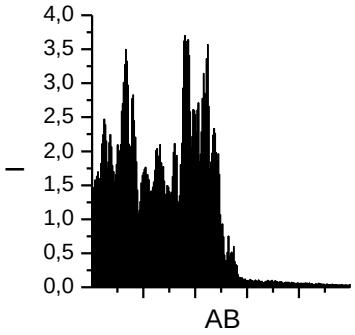	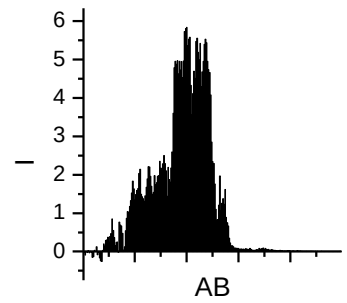	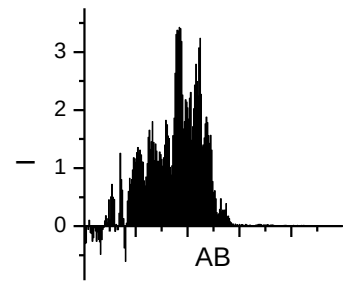
	*CIE-L**	*CIE-u**	*CIE-v**

In order to evaluate the reliability of picked stages, average linear deviation, sample standard deviation and standard deviation of the bias-corrected variance were found. The modification of neither MPA nor GT within reasonable limits proved to be needless, as the mentioned parameters hardly changed in the observed interval, whereas the change of CT1 or CT2 allowed providing reliable calculations. The statistical data, provided by varying CT1 turned out to be higher than CT2, so only data for CT1 is displayed in Table 3.

Average linear deviation:

$$d = \frac{\sum |x_i - \bar{x}|}{n} \quad (2)$$

Sample standard deviation:

$$\sigma = \sqrt{\frac{1}{n}\sum_{i=1}^{n}(x_i - \bar{x})^2} \quad (3)$$

TABLE III. STATISTICAL GROUND OF THE SEPARATION PROCESS

CT1	Stage	Red		Yellow		Magenta		RYM average differences	
		$d \cdot 10^2$	$\sigma \cdot 10^2$	$d \cdot 10^2$	$\sigma \cdot 10^2$	$d \cdot 10^2$	$\sigma \cdot 10^2$	$\Delta d \cdot 10^4$	$\Delta\sigma \cdot 10^4$
50	1	4.99	6.6	3.43	6.11	1.36	1.74	7.09	7.28
	2	2.28	3.09	6.26	6.36	4.84	5.37	2.77	7.96
	3	3.44	4.19	1.33	1.51	5.35	6.74	3.63	1.91
45	1	5.58	6.98	3.22	4.86	1.65	2.03	1.40	2.44
	2	2.38	3.52	5.89	6.64	5.07	5.68	5.44	3.06
	3	3.61	3.96	1.69	1.77	6.88	7.99	1.49	6.13
40	1	5.34	7.12	5.37	6.25	2.3	2.57	6.36	4.19
	2	2.39	3.46	6.23	6.51	4.8	4.98	1.81	-0.51
	3	3.75	4.55	1.75	1.87	7.09	8.71	3.45	1.98
35	1	5.48	7.26	5.44	5.86	2.56	2.9	3.83	3.87
	2	3.11	4.15	6.04	6.28	4.92	5.3	2.04	6.36
	3	3.47	4.05	1.57	1.68	6.62	7.95	4.37	0.88
30	1	5.52	7.5	5.03	5.6	3.62	4.21	2.14	0.53
	2	3.7	4.54	5.81	6.55	4.4	5.03	6.27	3.52
	3	3.12	3.97	1.82	2.36	6.12	7.58	1.50	2.63
25	1	6.31	7.64	5.42	5.92	3.28	3.57	6.72	0.25
	2	4.39	5.15	6.86	7.91	4.58	5.24	3.87	5.88
	3	3.73	4.55	1.89	2.27	6.29	7.44	6.57	2.89
—	1	6.27	8.25	8.9	10.76	4.33	5.22	4.08	1.84
	2	8.9	10.76	7.33	8.22	6.6	7.45	4.65	0.68
	3	4.33	5.22	3.6	4.45	9.15	12.73	-1.82	0.54

It is seen that in general the larger the CT1 the smaller the error, yet the reliability is remained, due to small error values. The obtained color distribution after tracing (Figure 5) with good reliability proves the abrupt change in lignin mass content in the outer part of the agglomerate.

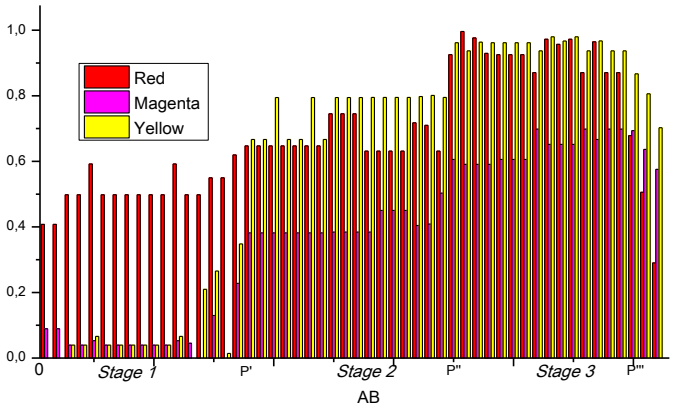

Figure 5. Modified Red, Magenta and Yellow distribution of the I part of the image

The set of 25 images was studied similarly. It was found, that the number of steps may vary, nevertheless, the frequency vary significantly (Figure 6). The tracing method was applied to rest of the values similarly as was described. This operation was performed to find the number of stages in agglomerate, given the fact that the physical properties within the agglomerate vary more monotonically than properties in the border parts, studied earlier in this research.

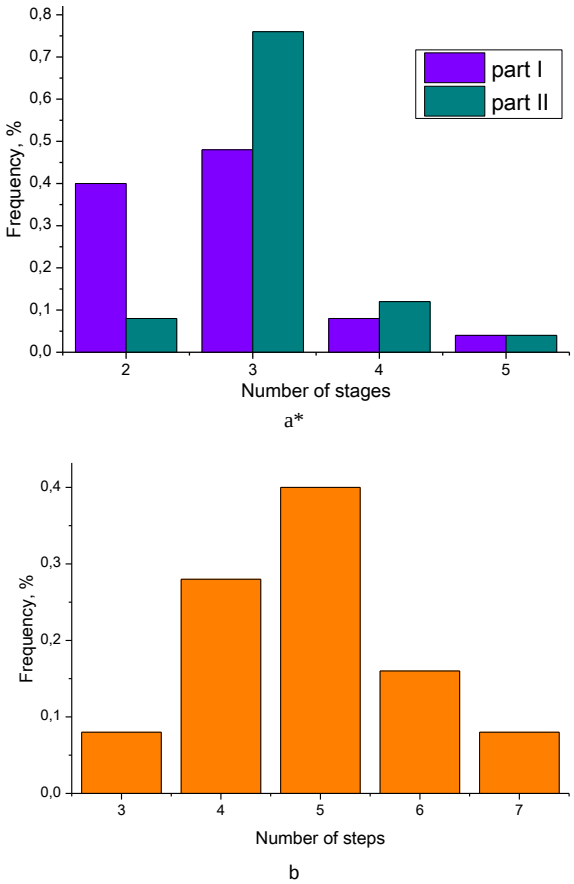

Figure 6. Number of stages for the investigated set (25 images). *For both parts, the list of stages included the stage with maximum value of *I*.

To find I in Beer-Lambert formula the average value was calculated. In all cases $I_1 = I_0, w_1 = 0$ according to experimental conditions. This allows calculating the lignin content in all stages using the formula:

$$\frac{I_{n-1}}{I_n} = \frac{I_o e^{-\chi_{\lambda_{n-1}} C_{n-1} l_{n-1}}}{I_o e^{-\chi_{\lambda_n} C_n l_n}} = e^{k_n - k_{n-1}} \quad (4)$$

$$k_i = \chi_{\lambda_i} C_i l_i = \chi_{\lambda_i} w_i l_i = f(w_i) \quad (5)$$

It was found that in different photos the mass content of lignin may vary, especially in the low lignin-content part of the agglomerate, whereas the content of lignin in the last stage remains the same, resulting 40.86±0.34 % (Figure 7). This data correlates with the capillary-saturated value for lignin-DF systems, founded earlier [17], proving the existence of capillary forces not only for colloid particle [18], but also within the agglomerate itself.

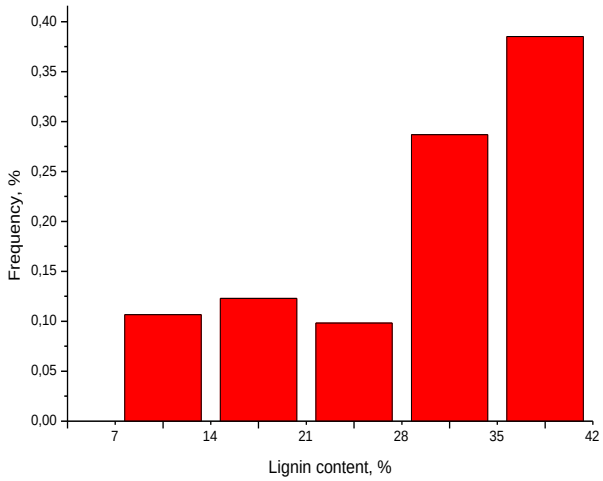

Figure 7. Lignin content distribution in the lignin – DF colloid aggregate

There is certain analogue between the way the lignin content changes within the colloid particle and the ζ-potential (zeta-potential) change in the electrical double layer of a charged particle. The Stern layer (negative charges in Figure 8) represents the center of the agglomerate, whereas Gouy-Chapman layer primarily stands for part II. The measured ζ-potential of lignin in diesel fuel is –24.10±1.26 mV, what can be explained by low dissociation of different functional groups presented in lignin. ζ-potential represents repulsive electrostatic forces between the lignin particles compensated by Van der Waals and strong hydrophobic forces that are favored, due to high concentration of hydrocarbon products in diesel fuel, what result in a stable lignin-DF dispersion. So the structure of the lignin agglomerate proved to be similar to another colloid particle-micelle, however, without a clearly marked separation of charges [19] (Figure 8).

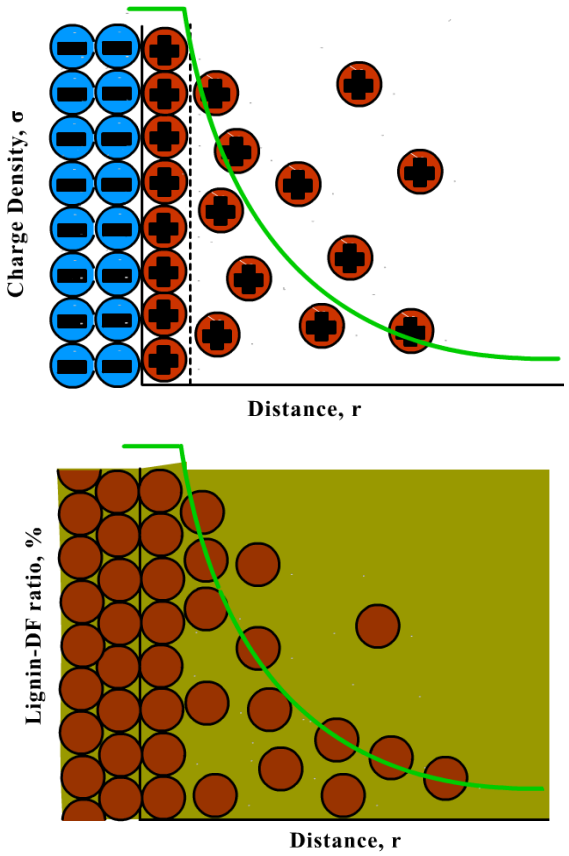

Figure 8. The similarity of the charge density – distance and lignin – DF ratio for micelles and colloid aggregates respectively

High continuity of lignin-DF dispersions at ratios, close to 40.86±0.34% is firstly explained by strong capillary forces presented in the nuclei of the lignin agglomerate. The behavior of lignin-DF dispersion is opposite to aqueous lignin solution, described earlier [20], due to different solvent polarities.

A fractal aggregation model was suggested earlier for kraft lignin [21]. As it is seen from microphotographs (Figure 2), colloid particles are spherical, adapting very compact conformations due to high molecular weight fragments and the cross-linked structure [22]. In terms of classical diffusion limited aggregation (DLA) theory a separate particle (released from a random place) is immediately attached to the cluster. Modified theory [23] includes a "sticking coefficient" or "sticking probability"-the probability for the particle to be attached to the cluster. As it can be seen on Figure 9, sticking coefficient (K_{st}) influences on the nominal aggregates density, measured as the ratio of the logarithms of the amount of particles in the aggregate to the radius of the aggregate. According to Figure 2, it may be said, that the nuclei of the aggregate has a low sticking coefficient, whereas the outer border of the aggregate is blurred. The estimated K_{st} for described system is between 0.01-0.1, more likely 0.02-0.05.

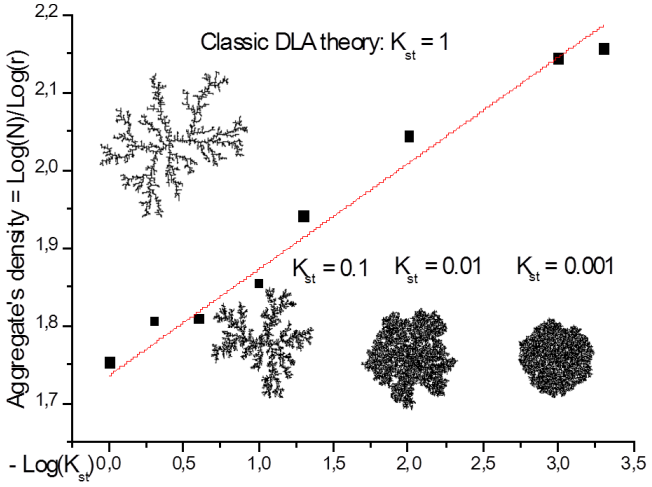

Figure 9. Dependence of the nominal aggregate's density and sticking coefficient

Figure 2a and Figure 10c represents the idea of considering aggregation process in terms of nucleation, where the nucleation process is followed by the colloid particle growth process that is kinetically slower and allows particles to aggregate at low lignin contents as independent spherical particles to form at high lignin contents a spatial grid.

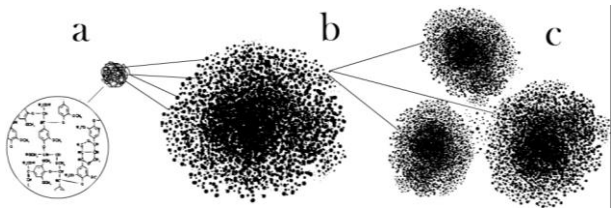

Figure 10. a: individual macromolecular colloid particle, b: individual colloid aggregate, c: spatial grid of colloid aggregates

In addition the continuity of lignin-DF dispersion at ratios, close to 40.86±0.34% not typical for most of the sorbents can be explained by the absence of voids, inherent for dispersions with fractal particle growth (Figure 10). The similarity between

The aggregation process can also be seen on SEM photographs. It is clear that for systems with higher DF content, the particles seem to be united into greater formations (Figure 11).

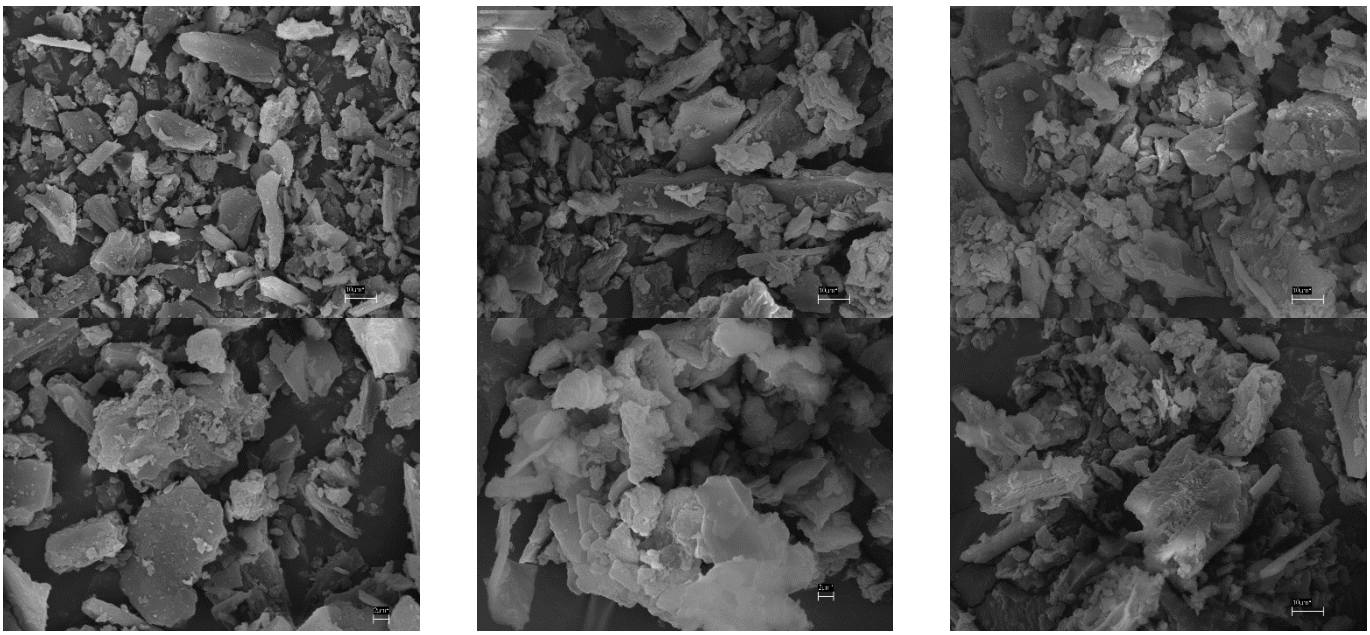

a *b* *c*

Figure 11. SEM photographs of lignin-DF dispersion with lignin content a: 100%, b: 66%, c: 50%.

IV. Conclusions

The method of photogrammetry was first used to study colloid aggregates. A set of 25 images of lignin-in-DF colloid particles was analyzed with further distinguishing by three main color intensities (Red, Magenta, Yellow), that are specific for studied colloid system, the layer structure of the agglomerates was proved. By stage separating the number of layers on a par with the ratio of the components of the colloid system was calculated for a set of 25 images. Certain correlation was found between the investigated colloid

aggregates and micelle structures. The obtained content of the dispersed phase 40.86±0.34 % correlates with capillary-saturated ratio for the studied systems. The nuclei of the aggregate found to have a low sticking coefficient, whereas the outer border of the aggregate is blurred, allowing correlating the experiment with the diffusion limited aggregation theory. The aggregation process was also noted on the SEM photographs, though for limited range of lignin concentrations.

V. APPENDIX: THE CODE

```
public class RGB_Diagonal_Analysis {
  public static void main(String[] foo) {
    new RGB_Diagonal_Analysis();
  }
  public void marchThroughImage(BufferedImage image) {
    int w = image.getWidth();
    int h = image.getHeight();
        int n_step = 100;
        int y;
        int x;
        System.out.println("width, height: " + w + ", " + h);

        PrintWriter Doc = null;
        try{
        Doc = new PrintWriter(new
FileOutputStream("pixels_file_25_50.txt"));
      for(int i = 0; i < n_step+1; i++) {

                    try{
                    y = i*h/n_step;
                    x = w-i*w/n_step;
                    System.out.println(i+1);
                    System.out.println("x,y: " + x + ", " + y);
        int pixel = image.getRGB(x, y);
                    int red = (pixel >> 16) & 0xff;
                    int green = (pixel >> 8) & 0xff;
                    int blue = (pixel) & 0xff;
                    System.out.println("rgb: " + red + ":" + green +
":" + blue);
                    Doc.println("x,y: " + x + ", " + y+":rgbcmy: " +
red + ":" + green + ":" + blue );
                    }
                    catch(ArrayIndexOutOfBoundsException e)
                    {
                    System.out.println("Done");
                    }

    }
    Doc.close();
    }
    catch(FileNotFoundException e)
      {
          System.out.println("Cannot load file pixels_file.txt");
           System.exit(0);
      }
          }
    public RGB_Diagonal_Analysis() {
      try {
        // get the BufferedImage, using the ImageIO class
        BufferedImage image =

ImageIO.read(this.getClass().getResource("25_50_n_n.png"));
        marchThroughImage(image);
          }
          catch (IOException e) {
        System.err.println(e.getMessage());
      }
    }
  }
```

REFERENCES

[1] Drury, S. A., & Drury, S. A. (2001). Image interpretation in geology

[2] Paine, D. P., & Kiser, J. D. (2003). *Aerial photography and image interpretation*. John Wiley & Sons.

[3] Giger M. L., Karssemeijer N., Schnabel J. A. Breast image analysis for risk assessment, detection, diagnosis, and treatment of cancer //Annual review of biomedical engineering. – 2013. – Т. 15. – С. 327-357.

[4] Di Mario, C., Görge, G., Peters, R., Kearney, P., Pinto, F., Hausmann, D & Erbel, R. (1998). Clinical application and image interpretation in intracoronary ultrasound. *European heart journal*, *19*(2), 207-229

[5] Wyatt, C. C., & Pharoah, M. J. (1997). Imaging techniques and image interpretation for dental implant treatment. *The International journal of prosthodontics*, *11*(5), 442-452.

[6] Stokes, D. J. (2003). Recent advances in electron imaging, image interpretation and applications: environmental scanning electron microscopy. *Philosophical Transactions of the Royal Society of London. Series A: Mathematical, Physical and Engineering Sciences*, *361*(1813), 2771-2787.

[7] Lin, D. T. (2010). Autonomous sub-image matching for two-dimensional electrophoresis gels using MaxRST algorithm. *Image and Vision Computing*,*28*(8), 1267-1279.

[8] Prakoonwit, S., & Benjamin, R. (2007). 3D surface point and wireframe reconstruction from multiview photographic images. *Image and Vision Computing*,*25*(9), 1509-1518.

[9] Semmlow, J. L. (2011). Biosignal and medical image processing. CRC press.

[10] Artyushkova, K., Pylypenko, S., Dowlapalli, M., & Atanassov, P. (2012). Use of digital image processing of microscopic images and multivariate analysis for quantitative correlation of morphology, activity and durability of electrocatalysts.*RSC Advances*, *2*(10), 4304-4310.

[11] Olech, M., Komsta, Ł., Nowak, R., Cieśla, Ł., & Waksmundzka-Hajnos, M. (2012). Investigation of antiradical activity of plant material by thin-layer chromatography with image processing. *Food Chemistry*, *132*(1), 549-553.

[12] Wu, D., & Sun, D. W. (2013). Colour measurements by computer vision for food quality control–A review. Trends in Food Science & Technology, 29(1), 5-20.

[13] Sonka, M., Hlavac, V., & Boyle, R. (2014). Image processing, analysis, and machine vision. Cengage Learning.

[14] Leon, K., Mery, D., Pedreschi, F., & Leon, J. (2006). Color measurement in L∗ a∗ b∗ units from RGB digital images. Food research international, 39(10), 1084-1091.

[15] Hong, G., Luo, M. R., & Rhodes, P. A. (2001). A study of digital camera colorimetric characterisation based on polynomial modelling

[16] Kralchevsky, P. A., & Denkov, N. D. (2001). Capillary forces and structuring in layers of colloid particles. *Current Opinion in Colloid & Interface Science*, *6*(4), 383-401.

[17] Reznikov, I, Savitskaya, T. Structure and properties of lignin dispersions in petroleum products, Belarusian State University student conference. 2013

[18] Birdi, K. A. S. (Ed.). (2008). Handbook of surface and colloid chemistry. CRC Press

[19] Shchukin, E. D., Pertsov, A. V., & Amelina, E. A. (1982). Colloid chemistry

[20] Wang, G. & Chen, H. 2013. Fractionation of alkali-extracted lignin from steam-exploded stalk by gradient acid precipitation. Separation and Purification Technology, 105, 98-105

[21] Norgren, M., Edlund, H., & Wågberg, L. (2002). Aggregation of lignin derivatives under alkaline conditions. Kinetics and aggregate structure. *Langmuir*, *18*(7), 2859-2865

[22] Goring, D. A. I. In Lignin : Properties and Material; Glasser, W. G., Sarkanen, S., Eds.; ACS Symposium Series Vol. 397; American Chemical Society: Washington, DC, 1989; pp 2-10

[23] Hashim, M., & Thomas, P. I. (2012). Computational Analysis of Diffusion as a Stochastic System. Washington University in St. Louis Department of Physics, 27.